Effects of Heme Pocket Structure and Mobility on Cytochrome *c* Stability†

Xin Wen,‡ Kirti M. Patel, Brandy S. Russell,§ and Kara L. Bren*

Department of Chemistry, University of Rochester, Rochester, New York 14627-0216

Received November 16, 2006; Revised Manuscript Received December 19, 2006

ABSTRACT: Unfolding thermodynamics of a thermophilic cytochrome c_{552} from *Hydrogenobacter thermophilus* (*Ht* cyt c_{552}) and its mesophilic homologue from *Pseudomonas aeruginosa* (*Pa* cyt c_{551}) as well as two heme pocket point mutants (*Ht*-Q64N and *Pa*-N64Q) are characterized by determination of protein stability curves (plots of unfolding free energy, ΔG, vs T). These proteins show revealing differences in heme pocket hydrogen bonding and mobility. It previously has been shown that Asn64 in *Pa* cyt c_{551} and in *Ht*-Q64N interacts with the heme axial Met to fix it in a single conformation [Wen, X., and Bren, K. L. (2005) *Biochemistry 44*, 5225−5233]. In *Ht* cyt c_{552} and *Pa*-N64Q, Gln64 does not interact with the axial Met; in these variants the axial Met samples more than one conformation [Wen, X., and Bren, K. L. (2005) *Inorg. Chem. 44*, 8587−8593]. Here it is demonstrated that, relative to wild type, *Pa*-N64Q displays enhanced stability with an increase in unfolding free energy ($\Delta\Delta G$) of 7.1 kJ/mol and an increase in denaturation temperature (ΔT_m) of 8 °C. Correspondingly, *Ht*-Q64N is less stable than *Ht* cyt c_{552}, with a $\Delta\Delta G$ of −10 kJ/mol and a ΔT_m of −10 °C. Analysis of unfolding thermodynamics indicates that the net changes in stability resulting from the position 64 mutations are primarily attributable to entropic factors. For *Pa*-N64Q (*Ht*-Q64N) it is proposed that the favorable release (unfavorable burial) of residue 64 is the dominant factor impacting stability. The mobility of the axial Met also is proposed to contribute. These results provide a specific illustration of how amino acid side chain mobility and burial or release contribute to protein stability.

Thermophilic proteins are more resistant to denaturation than mesophilic homologues, although thermophile/mesophile homologue protein pairs generally have similar sequences and structures (*1*, *2*). Delineating the factors accounting for differences in stability between protein homologues has been a goal in the field of protein structure and folding. One approach to investigating this problem is to compare the thermodynamics of unfolding of a thermophilic protein and its mesophilic counterpart directly. For example, there have been such comparative studies on α-amylases (*3*), phycocyanins (*4*), ribonucleases H (*5*), histidine-containing phosphocarrier proteins (*6*), and cytochromes *c* (cyts *c*)[1] (*7*). Several factors have been proposed to play roles in stabilizing proteins from thermophiles relative to their less stable homologues including increased packing density and hydrophobic interactions, more ion pairs, enhanced hydrogen bonding, and decreased flexibility (*8*−*12*). Complementing studies of protein homologues, site-directed mutagenesis is useful for elucidating contributions of specific interactions to protein stability. Studies have shown that the stability of mesophilic proteins can in some cases be increased by substituting one or more residues from the sequence of a thermophilic homologue (*13*−*16*).

One thermophile/mesophile pair that has been a valuable model system in comparative studies of protein stability is cyt c_{552} from the thermophile *Hydrogenobacter thermophilus* (*Ht*) and cyt c_{551} from mesophile *Pseudomonas aeruginosa* (*Pa*) (*17*). These homologues are members of the cyt c_8 structural family and have His-Met heme axial ligation (*18*, *19*). Despite high similarity in three-dimensional structure (*20*−*22*) and sequence (70% similarity), *Ht* cyt c_{552} is substantially more resistant to thermal denaturation than is *Pa* cyt c_{551} (*7*, *23*). Another important difference between *Ht* cyt c_{552} and *Pa* cyt c_{551} is revealed by their ^{1}H NMR hyperfine shift patterns in the oxidized, paramagnetic ($S = {}^1/_2$) state (*24*). The difference in heme electronic structure observed through NMR is attributed to a difference in the orientation and dynamics of the heme axial Met between *Ht* cyt c_{552} and *Pa* cyt c_{551}: The heme axial Met in *Pa* cyt c_{551} has the conformation seen for most cyts c_8, resulting in the pattern of paramagnetic heme methyl shifts for the ferric protein typical of this family (*25*), whereas in *Ht* cyt c_{552} the axial Met side chain (Figure 1) undergoes microsecond time scale motion proposed to be inversion at δS, resulting in an unusual, compressed heme methyl shift pattern (*26*).

To better understand the structural basis for the different axial Met behaviors in these proteins, mutations were introduced for the "distal" heme pocket residue 64 (number-

† This work supported by National Institutes of Health Grant GM63170. K.L.B. acknowledges an Alfred P. Sloan Research Fellowship.

* To whom correspondence should be addressed. Telephone: (585) 275-4335. Fax: (585) 276-0205. E-mail: bren@chem.rochester.edu.

‡ Current address: Department of Chemistry and Biochemistry, California State University, Los Angeles, CA 90032.

§ Current address: Department of Chemistry, Gustavus Adolphus College, St. Peter, MN 56082.

[1] Abbreviations: CD, circular dichroism; cyt *c*, cytochrome *c*; *Ht* cyt c_{552}, *Hydrogenobacter thermophilus* cytochrome c_{552}; *Ht*-Q64N, *Hydrogenobacter thermophilus* Gln64 → Asn cytochrome c_{552}; NMR, nuclear magnetic resonance; NOE, nuclear Overhauser effect; *Pa* cyt c_{551}, *Pseudomonas aeruginosa* cytochrome c_{551}; *Pa*-N64Q, *Pseudomonas aeruginosa* Asn64 → Gln cytochrome c_{551}.

10.1021/bi602380v CCC: $37.00
Published on Web 02/06/2007

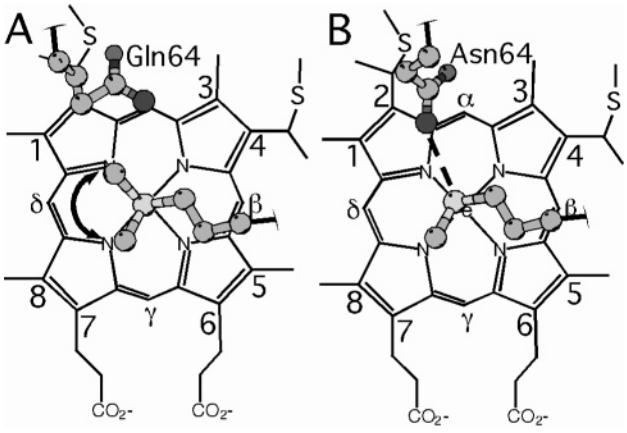

FIGURE 1: Positions of residues 61 and 64 in (A) *Ht* cyt *c* and (B) *Pa* cyt *c* relative to heme. The axial Met61 is fluxional in *Ht* cyt *c*. The dashed line indicates the Asn64 δNH interaction with Met61 δS. The heme pocket of *Pa*-N64Q resembles that of *Ht* cyt *c*, and *Ht*-Q64N resembles *Pa* cyt *c* (*27*, *28*).

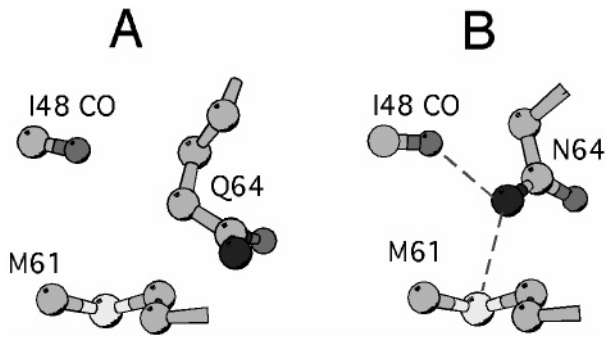

FIGURE 2: Interactions between key heme pocket residues in (A) *Ht* cyt *c* [PDB identifier 1YNR (*22*)] and (B) *Pa* cyt *c* [PDB identifier 351C (*20*)]. The Met61 orientation observed in *Pa* cyt *c* and in *Ht*-N64Q (*27*) is shown in (A) to facilitate comparison. Dashed lines indicate proposed hydrogen-bonding interactions.

ing based on *Pa* cyt c_{551} sequence), which is Asn in *Pa* cyt c_{551} and in most members of the cyt c_8 family, but Gln in *Ht* cyt c_{552}, creating the mutants *Ht*-Q64N (*27*) and *Pa*-N64Q (*28*). Despite the conservative nature of this substitution, Gln64 in *Ht* cyt c_{552} and Asn64 in *Pa* cyt c_{551} exhibit substantially different positions within the heme pocket. The Gln64 side chain in *Ht* cyt c_{552} (*22*) [and in *Pa*-N64Q (*28*)] is oriented toward the protein surface and does not interact with other heme pocket residues. The Asn64 side chain in *Pa* cyt c_{551} (*20*) [and in *Ht*-Q64N (*27*)] is oriented toward the heme center, positioned to interact with the axial Met61 δS as well as the backbone carbonyl oxygen of Ile48 in the heme pocket (Figures 1 and 2) (*20*−*22*, *27*, *28*). Accompanying differences in residue 64 orientation are differences in axial Met orientation and dynamics. In *Ht* cyt c_{552} and *Pa*-N64Q, the axial Met displays fluxional behavior, sampling two configurations, whereas in *Pa* cyt c_{551} and *Ht*-Q64N, the axial Met is fixed in one position (Figure 1). The difference in behavior of the axial Met results in the different heme electronic structures reflected by the ^{1}H NMR spectra of the oxidized proteins and plays a role in tuning redox potential (*26*−*30*).

Previous studies of the position 64 mutants of these cyts c_8 established the importance of an amino acid in contact with the heme axial Met for determining heme electronic structure and redox potential (*27*, *28*, *30*), but the effects of such altered heme pocket interactions on protein stability also are of interest. There is precedent for the substitution of amino acids from the sequence of a thermophilic protein into that of a homologous mesophilic protein to successfully enhance stability (*13*−*15*, *31*−*33*). The different heme pocket structures for *Ht* cyt c_{552} and *Pa* cyt c_{551}, in particular in the positions of residue 64, raise interesting questions relevant to understanding protein stability. Introduction of the N64Q mutation in *Pa* cyt c_{551} substitutes a residue in the mesophilic protein with one from its thermophilic homologue, which in a number of cases is found to be stabilizing (*15*, *17*, *31*). However, this mutation results in disruption of hydrogen-bonding interactions within the heme pocket (Figure 2) (*28*), which is expected to be destabilizing. Conversely, mutating Gln64 to Asn in *Ht* cyt c_{552} places a residue from the mesophilic protein sequence (Asn64) into the thermophile and results in enhanced hydrogen bonding within the heme pocket (*27*). Is this a case where introducing a residue from a mesophile into a thermophile will *enhance* thermophilic protein stability by improving hydrogen-bonding interactions? Here, the question of how heme pocket interactions involving residue 64 affect stability of these proteins is addressed through thermal and chemical denaturation studies of *Ht* cyt c_{552}, *Ht*-Q64N, *Pa* cyt c_{551}, and *Pa*-N64Q. The resulting protein stability curves (*34*) have been determined, and thermodynamic parameters for unfolding of the two mutants are compared with those for the wild-type proteins. In addition, comparisons of global structure and dynamics by NMR are included to aid interpretation of the results.

MATERIALS AND METHODS

Protein Sample Preparation. Recombinant *Ht* cyt c_{552}, *Ht*-Q64N, *Pa* cyt c_{551}, and *Pa*-N64Q and uniformly ^{15}N-labeled *Ht* cyt c_{552}, *Ht*-Q64N, and *Pa*-N64Q, were expressed and purified as previously described (*24*, *27*, *28*, *35*). Protein concentrations were determined using extinction coefficients of 105 mL mol^{-1} cm^{-1} at 409.5 nm for *Ht* cyt c_{552} and *Ht*-Q64N (*24*) and 106 mL mol^{-1} cm^{-1} at 410 nm for *Pa* cyt c_{551} and *Pa*-N64Q (*36*). Absorption measurements were carried out using a Shimadzu UV-2401PC photometer unit and a 1.000 cm path-length quartz cell. Unless indicated otherwise, all proteins were used in their oxidized forms.

Chemical and Thermal Denaturations. Guanidine hydrochloride (GuHCl; Sigma or GE Healthcare, highest purity) was used as the denaturant in chemical unfolding experiments. The concentrations of stock solutions of GuHCl (~8 M GuHCl in 50 mM sodium phosphate buffer, pH 7.0) were determined using refractive index measured on a Bausch and Lomb Abbe refractometer (*37*). Circular dichroism (CD) spectroscopy was performed on an Aviv Instruments CD model 202 or on a JASCO 710 spectropolarimeter. CD instruments were equipped with jacketed cell holders connected to a circulating water bath, and quartz cells with 0.100 cm path length were used. For GuHCl denaturation experiments, protein samples contained 10 μM protein and varied (0−8 M) concentrations of GuHCl in 50 mM sodium phosphate buffer. The pH was adjusted to 7.0 by the addition of a small amount of sodium hydroxide solution to each sample. The denaturant concentration of each sample was determined by refractive index measurement. CD spectra of protein samples (200−240 nm) as a function of [GuHCl]

were recorded with an averaging time of 5 s (Aviv) or 2 s (JASCO) and a bandwidth of 1.00 nm. CD spectra of reference samples (buffer with 0−8 M GuHCl) were recorded under the same conditions to provide a baseline for subtraction from the spectra of the corresponding protein samples. The denaturation of protein samples was followed by the change of the CD signal at 222 nm. GuHCl denaturation experiments were performed at nine temperatures (10, 15, 20, 25, 30, 35, 40, 45, 50 °C) to aid the determination of the temperature dependence of unfolding free energy. For thermal denaturation experiments, the CD signal at 222 nm was recorded every 2.5 °C with a 1 min equilibration time at each temperature over the temperature range 10−90 °C. Thermal denaturation experiments in the presence of GuHCl were carried out in the presence of 0.6−1.2 M GuHCl for *Pa* cyt c_{551} and *Pa*-N64Q and in the presence of 3.2−3.8 M GuHCl for *Ht* cyt c_{552} and *Ht*-Q64N. Reversibility of unfolding was verified by returning denatured samples to room temperature, removing denaturant, and verifying that the CD spectrum is substantially the same as that of the native protein.

Denaturation and Stability Curve Data Analyses. Chemical denaturation curves were obtained by plotting the processed CD signals at 222 nm as a function of [GuHCl]. The fraction of unfolded protein was plotted as a function of temperature for thermal unfolding curves (examples shown in Figure 3). Both the thermal and chemical denaturation curves were analyzed using a two-state model (*37*). To determine denaturation temperatures, T_m, thermal unfolding data obtained as a function of [GuHCl] were analyzed by the linear extrapolation method (LEM) (*38*, *39*) using the equation

$$\Delta G_m = \Delta H_m - T_m \Delta S_m \quad (1)$$

The T_m in the absence of denaturant was estimated from a linear extrapolation of the plot of T_m([GuHCl]) vs [GuHCl] to a [GuHCl] value of 0 M (*40*, *41*). GuHCl denaturation data on each protein at each temperature were analyzed using a nonlinear least-squares (NLLS) method (*42*). The unfolding free energy in the absence of denaturant [$\Delta G(H_2O)$] was determined by fitting the curves to the equation

$$y = [(y_f + m_f[\text{GuHCl}]) + (y_u + m_u[\text{GuHCl}])(e^{-\{(\Delta G(H_2O) - m[\text{GuHCl}])/RT\}})]/(1 + e^{-\{(\Delta G(H_2O) - m[\text{GuHCl}])/RT\}}) \quad (2)$$

where y_f, m_f, and y_u, m_u are the intercepts and slopes of the pre- and posttransition regions, respectively, and m is a measure of ΔG dependence on denaturant concentration (*38*). KaleidaGraph 3.5 (Synergy Software) was used to plot and fit the curves. In order to gauge the quality of the data, the linear extrapolation method (LEM) using eq 3 (*38*, *39*) was used to determine ΔG values for comparison to values determined using NLLS fitting.

$$\Delta G([\text{GuHCl}]) = \Delta G(H_2O) - m[\text{GuHCl}] \quad (3)$$

Results from both methods are compared in the Supporting Information, Table S1.

Protein stability curves (*34*) in the absence of GuHCl were constructed by plotting $\Delta G(H_2O)$ values determined from GuHCl denaturation (from eq 2) as a function of temperature. In addition, the extrapolated T_m values [at which $\Delta G(H_2O) = 0$; Figure 4] were included. By fitting the stability curves to the modified Gibbs−Helmholtz equation (eq 4), values of T_m, ΔH_m, and ΔC_p were determined; ΔS_m is determined using eq 1 with ΔG_m set to 0. This treatment assumes that ΔC_p is temperature-independent (*43*).

$$\Delta G(T) = \Delta H_m(1 - T/T_m) + \Delta C_p[(T - T_m) - T\ln(T/T_m)] \quad (4)$$

Reported errors in thermodynamic parameters are the errors obtained from the fits of experimental data to the appropriate equation. Errors in differences are estimated from the multiple measurements of these differences in this work.

NMR Spectroscopy. Two-dimensional NOESY and TOCSY spectra and assignment of ^{1}H NMR resonances for reduced *Ht* cyt c_{552}, *Ht*-Q64N, *Pa* cyt c_{551}, and *Pa*-N64Q were reported previously (*24*, *27*, *28*, *35*). For heteronuclear ^{1}H−^{15}N NOE measurements, ^{15}N-labeled samples of oxidized *Ht* cyt c_{552}, *Ht*-Q64N, or *Pa*-N64Q were prepared by expression on minimal (M9) medium containing $^{15}NH_4Cl$ as the sole nitrogen source and purified as described for the corresponding wild-type proteins (*24*, *35*). Protein samples for NMR were in 50 mM sodium phosphate, pH 6.0, with a 5-fold molar excess of $K_3[Fe(CN)_6]$. {^{1}H}−^{15}N NOE data were recorded at 298 K on a Varian INOVA 500 MHz spectrometer on 1.2−1.6 mM protein samples with and without proton saturation as described (*35*). NOEs were determined as the ratio of the peak intensities in spectra with and without saturation (eq 5), and the errors were determined from the measurements of the root-mean-square baseline noise as described in detail elsewhere (*44*). {^{1}H}−^{15}N NOE data on *Pa* cyt c_{551}, collected on a 500 MHz spectrometer, are available in the literature (*35*).

$$\text{NOE} = I_{sat}/I_{unsat} \quad (5)$$

Analysis of Protein Structures. Hydrogen atoms were added to the X-ray crystal structures of oxidized *Ht* cyt c_{552} [PDB identifier 1YNR (*22*)] and *Pa* cyt c_{551} [PDB identifier 351C (*20*)] using the CalcAtom command in the MOLMOL software package (*45*) to evaluate interactions in the heme pocket. Hydrogen bonds were considered if the distance between the hydrogen atom (H) of the donor (D) and the acceptor (A) atom was less than 3.0 Å and the angle of D−H···A was larger than 120° (*46*).

RESULTS

Analysis of Protein Backbone Structure and Dynamics. The overall molecular structures of *Ht*-Q64N and *Pa*-N64Q were compared to their respective wild-type proteins by analysis of chemical shift differences ($\Delta\delta$) between Hα protons of mutant and wild-type proteins (Figure S1 in Supporting Information). This analysis was performed on the reduced (diamagnetic) proteins assisted by data available from previous studies (*27*, *28*); $\Delta\delta$ values for the oxidized proteins were not evaluated because these mutations induce a change in electronic structure, complicating interpretation of chemical shift changes in the paramagnetic oxidized forms. The data indicate that the overall molecular structures of the wild-type proteins are maintained in the mutants with only a few structural changes in the region close to the substitution

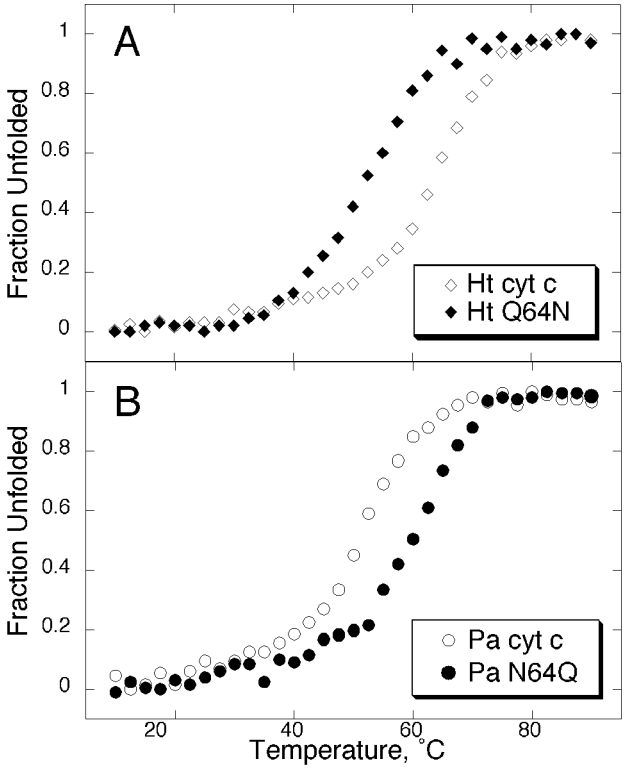

FIGURE 3: Thermal unfolding curves for (A) *Ht* cyt *c* (open diamonds) and *Ht*-Q64N (filled diamonds) in the presence of 3.6 M GuHCl and (B) *Pa* cyt *c* (open circles) and *Pa*-N64Q (filled circles) in the presence of 1.2 M GuHCl. *Ht*-N64Q and *Pa*-N64Q show a T_m decrease and increase, respectively, relative to wild type.

site. Evaluation of heme pocket structures of the oxidized proteins is available in the literature (*27*, *28*).

The fast backbone dynamics of the oxidized forms of the two mutants also were compared to those of the wild-type proteins by measuring $\{^1H\}-^{15}N$ NOEs, a sensitive indicator of fast internal motion (picosecond to nanosecond) (*47*) [data on *Pa* cyt c_{551} are available in the literature (*35*)]. Compared to the corresponding wild-type proteins, *Ht*-Q64N and *Pa*-N64Q show similar backbone amide heteronuclear NOE values overall, even near the mutation regions (Figure S2 in Supporting Information). This supports the proposal that differences in axial ligand dynamics between the proteins with Gln64 (*Ht* cyt c_{552}, *Pa*-N64Q) and those with Asn64 (*Pa* cyt c_{551}, *Ht*-Q64N) are confined to the amino acid side chain and do not significantly impact backbone dynamics.

GuHCl and Thermal Denaturations. Representative thermal unfolding curves for *Ht* cyt c_{552}, *Ht*-Q64N, *Pa* cyt c_{551}, and *Pa*-N64Q are shown in Figure 3. Thermal unfolding was performed in the presence of denaturant to allow observation of posttransition regions for all proteins; conditions were the same for the two members of each wild-type/mutant pair. The data clearly show that *Ht*-Q64N is less thermally stable than wild-type *Ht* cyt c_{552}; the T_m values from thermal unfolding in the presence of 3.5 M GuHCl for *Ht* cyt c_{552} and *Ht*-Q64N are 64 and 52 °C, respectively. *Pa*-N64Q, however, is more thermally stable than *Pa* cyt c_{551}; T_m values for *Pa*-N64Q and *Pa* cyt c_{551} in the presence of 1.0 M GuHCl are 65 and 57 °C, respectively. T_m values determined for the wild-type and mutant proteins from the thermal unfolding curves in the presence of various concentrations of GuHCl are reported in Figure 4. The data reveal that the mutation

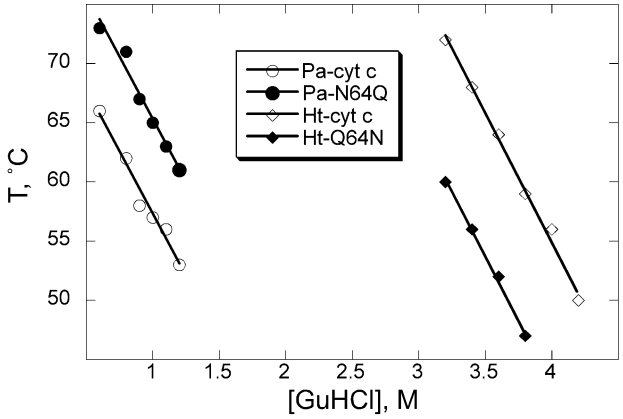

FIGURE 4: Plots of T_m as a function of [GuHCl] for *Ht* cyt *c* (open diamonds), *Ht*-Q64N (filled diamonds), *Pa* cyt *c* (open circles), and *Pa*-N64Q (filled circles).

Q64N in *Ht* cyt c_{552} results in a decrease in T_m of ~12 °C at each GuHCl concentration, whereas the mutation N64Q in *Pa* cyt c_{551} results in an increase in T_m of ~9 °C. The T_m values in the absence of denaturant for the four proteins were linearly extrapolated from the plots of the T_m values against the denaturant concentrations (*48*) and are 139 ± 4 °C for *Ht* cyt c_{552}, 129 ± 3 °C for *Ht*-Q64N, 80 ± 2 °C for *Pa* cyt c_{551}, and 88 ± 2 °C for *Pa*-N64Q. The extrapolated T_m of 80 °C for *Pa* cyt c_{551} compares well with reported T_m values of 85 and 82 °C (*7*, *23*). In contrast, there is disparity between the T_m value of 139 °C for *Ht* cyt c_{552} and the directly measured (under pressure) value of 110 °C (*23*). This may be a result of error introduced from the long extrapolation required to determine the T_m for *Ht* cyt c_{552} in the absence of denaturant or of different conditions under which these values were measured. The T_m values for the four proteins determined here are included in the protein stability curves (see below).

The temperature dependence of $\Delta G(H_2O)$, *m*-values, and $[GuHCl]_{1/2}$ ([GuHCl] for unfolding transition midpoint; Supporting Information, Tables S2 and S3) were determined from GuHCl denaturation curves by curve fitting to eq 2. The $\Delta G(H_2O)$ and $[GuHCl]_{1/2}$ values for *Ht*-Q64N are lower than those for *Ht* cyt c_{552} at all temperatures investigated, and the $\Delta G(H_2O)$ and $[GuHCl]_{1/2}$ values for *Pa*-N64Q are greater than those for *Pa* cyt c_{551} at all temperatures investigated. The *m*-values, describing the denaturant dependence of ΔG, are proportional to the change in solvent-accessible surface area of a protein upon unfolding (*49*). The four proteins have comparable *m*-values that do not change significantly with temperature: *Ht*-Q64N has slightly smaller *m*-values compared to those of *Ht* cyt c_{552}; *Pa*-N64Q has slightly larger *m*-values compared to *Pa* cyt c_{551}. The parameters determined using fitting to eq 2 are in good agreement with those determined from these curves by LEM (Table S1 in Supporting Information), indicating that the values determined are not sensitive to the data analysis method.

Stability Curves. Through plotting the free energy of unfolding in the absence of GuHCl as a function of temperature, stability curves for the two mutants and the two wild-type proteins were constructed (Figure 5). The T_m value of each protein (where $\Delta G = 0$) determined by extrapolation (Figure 4) was included for each fit. As expected, $\Delta G(H_2O)$ reaches a maximum value at a particular temperature (T_s)

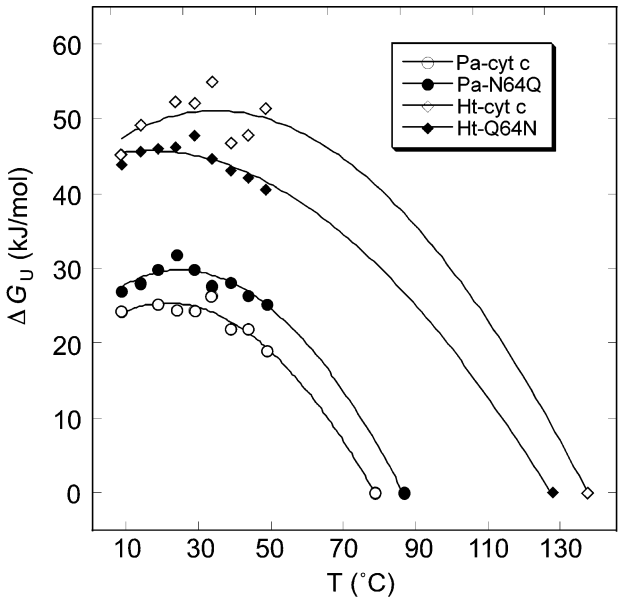

FIGURE 5: Protein stability curves for *Ht* cyt *c* (open diamonds), *Ht*-Q64N (filled diamonds), *Pa* cyt *c* (open circles), and *Pa*-N64Q (filled circles). The stability curves of the wild-type cyts *c* were plotted with the T_m values determined from thermal unfolding [T at $\Delta G(H_2O) = 0$]. The other points represent the $\Delta G(H_2O)$ values determined from chemical unfolding at the given temperatures.

Table 1: Thermodynamic Parameters for *Ht* Cyt c_{552}, *Ht*-Q64N, *Pa* Cyt c_{551}, and *Pa*-N64Q from Protein Stability Curves with T_m Determined in This Work

parameter	*Ht* cyt c_{552}	*Ht*-Q64N	*Pa* cyt c_{551}	*Pa*-N64Q
T_m (K)	412 ± 3	402 ± 2	353 ± 1	361 ± 1
T_m (°C)	139	129	80	88
ΔC_p (kJ/mol-K)	3.4 ± 0.5	2.4 ± 0.2	4.8 ± 0.5	5.0 ± 0.4
ΔH_m (kJ/mol)	393 ± 33	314 ± 14	301 ± 16	339 ± 13
ΔS_m [J/(mol·K)]	954 ± 80	781 ± 35	853 ± 45	939 ± 36
ΔT_m (K)		-10 ± 1		8 ± 1
$\Delta\Delta H_{80}$ (kJ/mol)		4.0 ± 1.0		-2.0 ± 0.1
$-T\Delta\Delta S_{80}$ (kJ/mol)		-14 ± 4		9.1 ± 0.4
$\Delta\Delta G_{80}$ (kJ/mol)		-10 ± 5		7.1 ± 0.5
T_s (K)	311	290	296	299

for each protein. The curves shown in Figure 4 represent the fits of the data to the modified Gibbs−Helmholtz equation (eq 4). Through these fits, thermodynamic parameters (ΔH_m and ΔC_p) were determined for each protein (Table 1). The thermodynamic parameters determined from the stability curves without T_m values included (data not shown) exhibit similar trends as those listed in Table 1 but have much larger errors, which is most likely due to the lack of data at higher temperatures. Inspection of the stability curves reveals that the curve for *Ht*-Q64N is shifted downward and to the left relative to that of the wild type. In other words, the maximum $\Delta G(H_2O)$ for the mutant is decreased, as is the temperature of maximum stability, T_s. Correspondingly, the stability curve for *Pa*-N64Q is shifted upward and slightly to the right compared with that of wild-type *Pa* cyt c_{551}.

To facilitate comparison of data among the four proteins in this study, the differences (mutant minus wild type) in thermodynamic parameters were calculated for all proteins using 80 °C, the melting temperature of *Pa* cyt c_{551}, as a reference temperature (Table 1). Utilizing a reference temperature near the melting temperature of the proteins being studied is commonly used in such comparisons as it minimizes errors resulting from extrapolation (*50*). The values of ΔH_{80}, ΔS_{80}, and ΔG_{80} were thus obtained for each protein using eqs 6 and 7, and results are listed in Table 1.

$$\Delta H(T) = \Delta H_m + C_p(T - T_m) \quad (6)$$

$$\Delta S(T) = \Delta S_m + C_p \ln(T/T_m) \quad (7)$$

The stabilizing (destabilizing) effect of the position 64 mutation on unfolding free energy for *Pa* cyt c_{551} (*Ht* cyt c_{552}) is similar in magnitude. The change in unfolding entropy is found to be the dominant factor contributing to the changes in unfolding free energies upon mutation in both cases, more than compensating for the changes in unfolding enthalpy.

DISCUSSION

Effects of Mutations on Molecular Structure and Backbone Dynamics. Inspection of the crystal structures of *Ht* cyt c_{552} (*22*) and *Pa* cyt c_{551} (*20*) reveals different side chain positions for residue 64 in these proteins. As shown in Figures 1 and 2, the side chain of Gln64 in *Ht* cyt c_{552} is oriented away from the heme iron and is partially exposed to solvent, whereas the side chain of Asn64 in *Pa* cyt c_{551} is buried in the heme pocket. There is only one hydrogen bond between Gln64 and other residues found in *Ht* cyt c_{552}: Gln64CO to Val66HN (2.92 Å heavy-atom distance). In contrast, in *Pa* cyt c_{551}, hydrogen bonds are found between Asn64 and a number of neighboring residues: Asn64HN to Lys49CO (2.35 Å) and to Ile48CO (2.98 Å), Asn64δH to Ile48CO (1.75 Å) and to Met61δS (2.78 Å), and Asn64CO to Val66HN (2.25 Å). Published analyses of the heme pocket structures of oxidized and reduced *Pa*-N64Q (*28*) and *Ht*-Q64N (*27*), performed through analysis of $^1H-^1H$ NOEs, heme ring current shifts, and pseudocontact shifts, reveal that the structure of the heme pocket of *Pa*-N64Q is similar to that of *Ht* cyt c_{552} (*28*) and also that the heme pocket of *Ht*-Q64N is similar to that of *Pa* cyt c_{551} (*27*). More specifically, the positions of the heme axial Met61 and of residue 64 in each of these pairs of proteins are very similar: The side chain of Asn64 in *Ht*-Q64N interacts with residues 61 and 48 as seen in *Pa* cyt c_{551}, whereas the Gln64 side chain in *Pa*-N64Q is oriented away from the heme pocket and is solvent exposed as in *Ht* cyt c_{552}.

To supplement these analyses and aid our interpretation of thermodynamic data on mutants, we performed a simple comparison of global structures of the mutants relative to the structures of the wild-type proteins by obtaining $\Delta\delta$ values [$\delta(H\alpha)$, mutant minus $\delta(H\alpha)$, wild type] for the reduced, diamagnetic proteins (*26*−*28*). In Figure S1, the differences in proton chemical shift of the backbone αH are compared for each mutant and its corresponding wild-type protein. Comparing the mutant and wild-type proteins, $\Delta\delta$ values are small (generally <0.1 ppm; systematic differences may be a result of referencing) throughout the structures except that large differences are observed for residue 64 (>0.7 ppm), the site of the mutation, as well as Ile48 (0.3 ppm) in the *Ht*-Q64N mutant, suggesting that residue 64 and its interaction with Ile48 are perturbed by mutation as expected (Figure 2). Typically, electron transfer proteins do not undergo significant changes in structure with redox state; thus, we will assume that the structures of the oxidized

proteins are similar to those of the reduced proteins. This assumption is supported by the observation of efficient electron transfer by these mutants (*30*), which is inconsistent with large redox-linked structure changes (*51*).

The position 64 mutations discussed here are known to impact heme axial Met dynamics (Figure 1) (*27*, *28*). To determine whether backbone dynamics also are affected, $\{^1H\}-^{15}N$ NOE values, which are sensitive to backbone motions on the picosecond to nanosecond time scale, were measured. As shown in Figure S2, the mutations do not significantly affect protein backbone motions to which this measurement is sensitive. Thus, differences in protein mobility resulting from the mutations are assumed to occur at protein side chains rather than the backbone, but a caveat is that the NOE experiment is not sensitive to slow motions.

Effects of Mutations on Unfolding Energetics. Despite the fact that the Asn64Gln mutation in *Pa* cyt c_{551} substitutes a residue from a thermophilic protein into a mesophilic protein, which often enhances stability (*31*), analysis of the structures of the wild-type and mutant proteins leads to the expectation that this substitution would decrease rather than enhance protein stability. This is because this substitution disrupts hydrogen-bonding interactions within the heme pocket (Figure 2). Interestingly, *Pa*-N64Q displays enhanced stability relative to the wild-type protein, as shown both by an elevated T_m and by a larger $\Delta G(H_2O)$ at all temperatures. An important indicator of the physicochemical basis for this stability enhancement comes from the thermodynamic parameters (Table 1), which reveal that enhancement of *Pa*-N64Q stability is a result of a decrease in unfolding entropy that more than compensates for a smaller decrease in unfolding enthalpy. As protein stability is determined by the sum of a large number of small favorable and unfavorable energetic factors, attributing such changes to specific interactions must be made with caution. Nevertheless, analysis of structure and dynamics of these proteins presented above supports the idea that these mutations exert primarily local effects and allow for such an analysis here.

The enhancement of stability via the entropic term may be a result of a net decrease in unfolded state entropy or a net increase in folded state entropy upon mutation (*52*, *53*). It is not expected that Asn/Gln substitutions would have a measurable impact on unfolded state entropy because of their similar properties in terms of effects on polypeptide mobility and solvation; thus we propose that an increase in folded state entropy occurs for *Pa*-N64Q. One effect that may account for this change is the release of the polar residue 64 from the heme pocket as a result of the Asn-to-Gln substitution, as Asn64 in these proteins is buried in the heme pocket but Gln64 is oriented away from the protein core and is solvent exposed (Figure 2). An estimate of the energetic cost paid for burying an Asn side chain at 80 °C is ~7.7 kJ/mol as a result of the entropy change associated with desolvation (*54*). A second, smaller, effect may be the axial Met, the side chain of which samples two conformations in the proteins that have Gln at position 64 (*Ht* cyt c_{552} and *Pa*-N64Q). This effect will increase folded state conformational entropy as estimated by the relationship in eq 8 (*55*), where *R* is the gas constant and *W* is the number of possible conformations:

$$T\Delta S_{conf} = TR \ln W = TR \ln 2 \quad (8)$$

At the reference temperature 80 °C, the increase in $-T\Delta S_{conf}$ for variants with Met sampling two conformations thus is estimated to be 2.0 kJ/mol. Although a small value, it is on the order of the contribution of a weak hydrogen bond (~2−6 kJ/mol) (*56*−*58*). It is notable that substituting Lys for Arg has similarly been proposed to enhance thermophilic protein stability by increasing folded state entropy as a result of the greater number of possible rotomers of Lys side chains relative to Arg in folded proteins (*53*).

The contributions of the release of residue 64 and mobility of residue 61 in *Pa*-N64Q relative to wild type provide a reasonable structural basis for the mutant's increase in stability driven by a decrease in unfolding entropy. One must also consider loss of a number of hydrogen-bonding interactions upon mutation which are expected to be destabilizing (by decreasing *H*). The small magnitude of the $\Delta\Delta H$ for *Pa*-N64Q may be a result of substitution of H-bonding with solvent for backbone atoms. Apparently, the factors discussed here, and likely other factors we have not identified that contribute to a net decrease in unfolding entropy in the mutant, more than compensate for the (small) decrease in unfolding enthalpy resulting from loss of hydrogen bonding within the heme pocket. The complementary arguments would hold for the basis for destabilization of *Ht*-Q64N relative to *Ht* cyt c_{552}, as the resulting thermodynamic parameters are similar in magnitude but opposite in direction to those obtained for *Pa*-N64Q relative to *Pa* cyt c_{551} (Table 1).

Relevance to Understanding Ht Cyt c_{552} Thermostability. Comparison of the thermodynamic parameters determined for *Ht* cyt c_{552} and *Pa* cyt c_{551} reveals that the thermophile utilizes both enthalpic and entropic factors to enhance stability; however, the entropic term is the larger in magnitude (Table 1). This observation is in agreement with a previous analysis of folding thermodynamics of these proteins that concluded that enhancement of *Ht* cyt c_{552} stability relative to *Pa* cyt c_{551} is through the entropic term (*15*). A number of specific factors have been identified as contributors to *Ht* cyt c_{552} thermostability in previous work in which stabilized mutants were made by substituting residues from the thermophile into the mesophile, resulting in enhanced hydrophobic and electrostatic interactions (*14*, *15*). Although the mutants reported previously show higher T_m values, their stability comes via an increase in ΔH, paying a cost with an increase in ΔS (*14*, *59*). Here, we demonstrate a specific substitution between these proteins that contributes to the entropic stabilization of the thermophile.

Summary. In this study, thermodynamic and structural bases are established for the significant stabilization seen for *Pa* cyt c_{551} upon mutation of Asn64 to Gln. The stability enhancement occurs despite the disruption of hydrogen-bonding interactions within the heme pocket and is attributed to a decrease in unfolding entropy for the mutant. In *Pa* cyt c_{551}, the polar residue Asn64 is anchored in the hydrophobic core by hydrogen bonds to compensate for the destabilizing dehydration effect of its burial (*60*). This allows a buried polar residue to interact with the heme axial Met, playing a role in tuning heme redox potential (*30*). In contrast, the smaller number of hydrogen bonds observed for Gln64 in *Pa*-N64Q (and *Ht* cyt c_{552}) is consistent with Gln64 being partially exposed to solvent. This result provides a specific example of the importance of entropic factors in determining

protein stability and also illustrates the importance of hydrogen-bonding interactions in stabilizing buried polar residues in protein active sites.

SUPPORTING INFORMATION AVAILABLE

One table comparing $\Delta G(H_2O)$ results from NLLS and LEM analysis, two tables listing $\Delta G(H_2O)$, *m*, and $[GuHCl]_{1/2}$ values, and figures comparing chemical shifts and backbone NOEs for wild-type and mutant proteins. This material is available free of charge via the Internet at http://pubs.acs.org.

REFERENCES

1. Razvi, A., and Scholtz, J. M. (2006) Lessons in stability from thermophilic proteins, *Protein Sci. 15*, 1569−1578.
2. Szilágyi, A., and Závodszky, P. (2000) Structural differences between mesophilic, moderately thermophilic and extremely thermophilic protein subunits: Results of a comprehensive survey, *Structure 8*, 493−504.
3. Fitter, J., and Haber-Pohlmeier, S. (2004) Structural stability and unfolding properties of thermostable bacterial alpha-amylases: A comparative study of homologous enzymes, *Biochemistry 43*, 9589−9599.
4. Roth, L. G., Berns, D. S., and Chen, C.-H. (1996) Comparative thermodynamic elucidation of the structural stability of thermophilic proteins, *Biophys. Chem. 60*, 89−97.
5. Hollien, J., and Marqusee, S. (1999) A thermodynamic comparison of mesophilic and thermophilic ribonucleases H, *Biochemistry 38*, 3831−3836.
6. Razvi, A., and Scholtz, J. M. (2006) A thermodynamic comparison of HPr proteins from extremophilic organisms, *Biochemistry 45*, 4084−4092.
7. Sanbongi, Y., Igarashi, Y., and Kodama, T. (1989) Thermostability of cytochrome *c*-552 from the thermophilic hydrogen oxidizing bacterium *Hydrogenobacter thermophilus*, *Biochemistry 28*, 9574−9578.
8. Vogt, G., Woell, S., and Argos, P. (1997) Protein thermal stability, hydrogen bonds, and ion pairs, *J. Mol. Biol. 269*, 631−643.
9. Zhou, H.-X. (2002) Toward the physical basis of thermophilic proteins: Linking of enriched polar interactions and reduced heat capacity of unfolding, *Biophys. J. 83*, 3126−3133.
10. Tang, K. E. S., and Dill, K. A. (1998) Native protein fluctuations: The conformational-motion temperature and the inverse correlation of protein flexibility with protein stability, *J. Biomol. Struct. Dyn. 16*, 397−411.
11. Kumar, S., Tsai, C.-J., and Nussinov, R. (2000) Factors enhancing protein thermostability, *Protein Eng. 13*, 179−191.
12. Kumar, S., Tsai, C. J., and Nussinov, R. (2001) Thermodynamic differences among homologous thermophilic and mesophilic proteins, *Biochemistry 40*, 14152−14165.
13. van den Burg, B., and Eijsink, V. G. H. (2002) Selection of mutations for increased protein stability, *Curr. Opin. Biotechnol. 13*, 333−337.
14. Hasegawa, J., Shimahara, H., Mizutani, M., Uchiyama, S., Arai, H., Ishii, M., Kobayashi, Y., Ferguson, S. J., Sambongi, Y., and Igarashi, Y. (1999) Stabilization of *Pseudomonas aeruginosa* cytochrome *c*-551 by systematic amino acid substitutions based on the structure of thermophilic *Hydrogenobacter thermophilus* cytochrome *c*-552, *J. Biol. Chem. 274*, 37533−37537.
15. Hasegawa, J., Uchiyama, S., Tanimoto, Y., Mizutani, M., Kobayashi, Y., Sambongi, Y., and Igarashi, Y. (2000) Selected mutations in a mesophilic cytochrome *c* confer the stability of a thermophilic counterpart, *J. Biol. Chem. 275*, 37824−37828.
16. Akanuma, S., Yamagishi, A., Tanaka, N., and Oshima, T. (1999) Further improvement of the thermal stability of a partially stabilized Bacillus subtilis 3-isopropylmalate dehydrogenase variant by random and site-directed mutagenesis, *Eur. J. Biochem. 260*, 499−504.
17. Sambongi, Y., Uchiyama, S., Kobayashi, Y., Igarashi, Y., and Hasegawa, J. (2002) Cytochrome *c* from a thermophilic bacterium has provided insights into the mechanisms of protein maturation, folding, and stability, *Eur. J. Biochem. 269*, 3355−3361.
18. Ambler, R. P. (1991) Sequence variability in bacterial cytochromes *c*, *Biochim. Biophys. Acta 1058*, 42−47.
19. Scott, R. A., and Mauk, A. G. (1996) *Cytochrome c: A Multidisciplinary Approach*, University Science Books, Sausalito, CA.
20. Matsuura, Y., Takano, T., and Dickerson, R. E. (1982) Structure of cytochrome *c*-551 from *Pseudomonas aeruginosa* refined at 1.6-Å resolution and comparison of the 2 redox forms, *J. Mol. Biol. 156*, 389−409.
21. Hasegawa, J., Yoshida, T., Yamazaki, T., Sambongi, Y., Yu, Y., Igarashi, Y., Kodama, T., Yamazaki, K., Kyogoku, Y., and Kobayashi, Y. (1998) Solution structure of thermostable cytochrome *c*-552 from *Hydrogenobacter thermophilus* determined by 1-H NMR spectroscopy, *Biochemistry 37*, 9641−9649.
22. Travaglini-Allocatelli, C., Gianni, S., Dubey, V. K., Borgia, A., Di Matteo, A., Bonivento, D., Cutruzzolà, F., Bren, K. L., and Brunori, M. (2005) An obligatory intermediate in the folding pathway of cytochrome *c*-552 from *Hydrogenobacter thermophilus*, *J. Biol. Chem. 280*, 25729−25734.
23. Uchiyama, S., Ohshima, A., Nakamura, S., Hasegawa, J., Terui, N., Takayama, S. I. J., Yamamoto, Y., Sambongi, Y., and Kobayashi, Y. (2004) Complete thermal unfolding profiles of oxidized and reduced cytochromes *c*, *J. Am. Chem. Soc. 126*, 14684−14685.
24. Karan, E. F., Russell, B. S., and Bren, K. L. (2002) Characterization of *Hydrogenobacter thermophilus* cytochromes *c*-552 expressed in the cytoplasm and periplasm of *Escherichia coli*, *J. Biol. Inorg. Chem. 7*, 260−272.
25. Senn, H., and Wüthrich, K. (1985) Amino acid sequence, heme iron coordination geometry and functional properties of mitochondrial and bacterial *c*-type cytochromes, *Q. Rev. Biophys. 18*, 111−134.
26. Zhong, L., Wen, X., Rabinowitz, T. M., Russell, B. S., Karan, E. F., and Bren, K. L. (2004) Heme axial methionine fluxionality in *Hydrogenobacter thermophilus* cytochrome *c*-552, *Proc. Natl. Acad. Sci. U.S.A. 101*, 8637−8642.
27. Wen, X., and Bren, K. L. (2005) Suppression of axial methionine fluxion in *Hydrogenobacter thermophilus* Gln64Asn cytochrome *c*-552, *Biochemistry 44*, 5225−5233.
28. Wen, X., and Bren, K. L. (2005) Heme axial methionine fluxion in *Pseudomonas aeruginosa* Asn64Gln cytochrome *c*-551, *Inorg. Chem. 44*, 8587−8593.
29. Bren, K. L., Kellogg, J. A., Kaur, R., and Wen, X. (2004) Folding, conformational changes, and dynamics of cytochromes *c* probed by NMR spectroscopy, *Inorg. Chem. 43*, 7934−7944.
30. Ye, T., Kaur, R., Wen, X., Bren, K. L., and Elliott, S. J. (2005) Redox properties of wild-type and heme-binding loop mutants of bacterial cytochromes *c* measured by direct electrochemistry, *Inorg. Chem. 44*, 8999−9006.
31. Lehmann, M., and Wyss, M. (2001) Engineering proteins for thermostability: the use of sequence alignments versus rational design and directed evolution, *Curr. Opin. Biotechnol. 12*, 371−375.
32. Clark, A. T., McCrary, B. S., Edmondson, S. P., and Shriver, J. W. (2004) Thermodynamics of core hydrophobicity and packing in the hyperthermophile proteins Sac7d and Sso7d, *Biochemistry 43*, 2840−2853.
33. Bonomi, F., Eidsness, M. K., Iametti, S., Kurtz, D. M., Mazzini, S., and Morleo, A. (2004) Contribution of the Fe-II(SCys)(4) site to the thermostability of rubredoxins, *J. Biol. Inorg. Chem. 9*, 297−306.
34. Becktel, W. J., and Schellman, J. A. (1987) Protein stability curves, *Biopolymers 26*, 1859−1877.
35. Russell, B. S., Zhong, L., Bigotti, M. G., Cutruzzolà, F., and Bren, K. L. (2003) Backbone dynamics and hydrogen exchange of *Pseudomonas aeruginosa* ferricytochrome *c*-551, *J. Biol. Inorg. Chem. 8*, 156−166.
36. Horio, T., Higashi, T., Sasagawa, M., Kusai, K., Nakai, M., and Okunuki, K. (1960) Preparation of crystalline *Pseudomonas* cytochrome *c*-551 and its general properties, *Biochem. J. 77*, 194−201.
37. Pace, C. N., and Sholtz, J. M. (1997) *Measuring the Conformational Stability of a Protein*, IRL, Oxford and New York.
38. Schellman, J. A. (1978) Solvent denaturation, *Biopolymers 17*, 1305−1322.
39. Greene, R. F., Jr., and Pace, C. N. (1974) Urea and guanidine hydrochloride denaturation of ribonuclease, lysozyme, agr-chymotrypsin, and β-lactoglobulin, *J. Biol. Chem. 249*, 5388−5393.

40. Pfeil, W., Gesierich, U., Kleemann, G. R., and Sterner, R. (1997) Ferredoxin from the hyperthermophile *Thermotoga maritima* is stable beyond the boiling point of water, *J. Mol. Biol. 272*, 591−596.
41. Wittung-Stafshede, P., Gomes, C. M., and Teixeira, M. (2000) Stability and folding of the ferredoxin from the hyperthermophilic archaeon *Acidianus ambivalens*, *J. Inorg. Biochem. 78*, 35−41.
42. Santoro, M. M., and Bolen, D. W. (1988) Unfolding free-energy changes determined by the linear extrapolation method. 1. Unfolding of phenylmethanesulfonyl α-chymotrypsin using different denaturants, *Biochemistry 27*, 8063−8068.
43. Nicholson, E. M., and Scholtz, J. M. (1996) Conformational stability of the *Escherichia coli* HPr protein: Test of the linear extrapolation method and a thermodynamic characterization of cold denaturation, *Biochemistry 35*, 11369−11378.
44. Farrow, N. A., Muhandiram, R., Singer, A. U., Pascal, S. M., Kay, C. M., Gish, G., Shoelson, S. E., Pawson, T., Formankay, J. D., and Kay, L. E. (1994) Backbone dynamics of a free and a phosphopeptide-complexed Src homology-2 domain studied by N-15 NMR relaxation, *Biochemistry 33*, 5984−6003.
45. Koradi, R., Billeter, M., and Wüthrich, K. (1996) MOLMOL: A program for display and analysis of macromolecular structures, *J. Mol. Graphics 14*, 51.
46. Ippolito, J. A., Alexander, R. S., and Christianson, D. W. (1990) Hydrogen bond stereochemistry in protein structure and function, *J. Mol. Biol. 215*, 457−471.
47. Kay, L. E., Torchia, D. A., and Bax, A. (1989) Backbone dynamics of proteins as studied by N-15 inverse detected heteronuclear NMR spectroscopy: Application to staphylococcal nuclease, *Biochemistry 28*, 8972−8979.
48. Pfeil, W., Gesierich, U., Kleemann, G. R., and Sterner, R. (1997) Ferredoxin from the hyperthermophile *Thermotoga maritima* is stable beyond the boiling point of water, *J. Mol. Biol. 272*, 591−596.
49. Myers, J. K., Pace, C. N., and Scholtz, J. M. (1995) Denaturant m-values and heat-capacity changes: Relation to changes in accessible surface areas of protein unfolding, *Protein Sci. 4*, 2138−2148.
50. Makhatadze, G. I., Loladze, V. V., Gribenko, A. V., and Lopez, M. M. (2004) Mechanism of thermostabilization in a designed cold shock protein with optimized surface electrostatic interactions, *J. Mol. Biol. 336*, 929−942.
51. Marcus, R. A., and Sutin, N. (1985) Electron transfers in chemistry and biology, *Biochim. Biophys. Acta 811*, 265−322.
52. Matthews, B. W., Nicholson, H., and Becktel, W. J. (1987) Enhanced protein thermostability from site-directed mutations that decrease the entropy of unfolding, *Proc. Natl. Acad. Sci. U.S.A. 84*, 6663−6667.
53. Berezovsky, I. N., Chen, W. W., Choi, P. J., and Shakhnovich, E. I. (2005) Entropic stabilization of proteins and its proteomic consequences, *PLoS Comput. Biol. 1*, 322−332.
54. Pickett, S. D., and Sternberg, M. J. E. (1993) Empirical scale of side-chain conformational entropy in protein folding, *J. Mol. Biol. 231*, 825−839.
55. Creighton, T. E. (1993) *Proteins: Structures and Molecular Properties*, W. H. Freeman, New York.
56. Fersht, A. R. (1985) Hydrogen bonding and biological specificity analysed by protein engineering, *Nature 314*, 235.
57. Fersht, A. R. (1987) The hydrogen bond in molecular recognition, *Trends Biol. Sci. 12*, 301−304.
58. Myers, J. K., and Pace, C. N. (1996) Hydrogen bonding stabilizes globular proteins, *Biophys. J. 71*, 2033−2039.
59. Uchiyama, S., Hasegawa, J., Tanimoto, Y., Moriguchi, H., Mizutani, M., Igarashi, Y., Sambongi, Y., and Kobayashi, Y. (2002) Thermodynamic characterization of variants of mesophilic cytochrome *c* and its thermophilic counterpart, *Protein Eng. 15*, 455−461.
60. Loladze, V. V., Ermolenko, D. N., and Makhatadze, G. I. (2002) Thermodynamic consequences of burial of polar and non-polar amino acid residues in the protein interior, *J. Mol. Biol. 320*, 343−357.

BI602380V